Journal of Fundamental and Applied Sciences

Research Article

ISSN 1112-9867

Available online at http://www.jfas.info

ADSORPTIVE REMOVAL OF METHYLENE BLUE DYE FROM SYNTHETIC WASTEWATER USING ACID AND BASE ACTIVATED *Adansonia digitata* SEED POD

Zahra'u Hashim[1*], Muhammad Bashir Ibrahim[1], Bishir Usman[1], Abdullahi Sulaiman Usman[2], Ayuba Abdullahi Muhammad[1]

[1]Department of Pure and Industrial Chemistry, Bayero University, P.M.B.3011, BUK, Kano-Nigeria

[2]Department of Chemistry, Faculty of Science, Yobe State University, Damaturu, Nigeria

Received: 02 August 2024 / Accepted: 23 Octobre 2024 / Published: 19 Decembre 2024

ABSTRACT

Using the batch adsorption method, the adsorption capacity of activated carbon from Adansonia digitata (AD) seed pods was investigated. Scanning electron microscopy (SEM) and Fourier transform infrared (FTIR) spectroscopy characterized the adsorbents. AD, HAD (H3PO4-activated AD), and KAD (KOH-activated AD) exhibited C-H, O-H, C≡N, and C=C groups with minor alterations post-activation and adsorption. The pH of point zero charge (pHpzc) for AD, HAD, and KAD were 6.6, 6.8, and 7.2, respectively. Optimized conditions included temperature, pH, adsorbent dosage, initial concentration, and agitation time. Maximum dye adsorption capacities on AD, HAD, and KAD were 91.48, 71.70, and 75.52 mg/g, respectively. Adsorption followed a pseudo-second-order model, and the Freundlich isotherm model correlated well. Thermodynamic studies indicated exothermic and spontaneous adsorption processes, suggesting these adsorbents are promising for industrial wastewater cleanup.

Keywords: Adsorption; Adsorbate; cationic dye; Kinetics; Isotherm; Thermodynamic.

Author Correspondence, e-mail: zaharahasheem61@gmail.com

doi: http://dx.doi.org/10.4314/jfas.1379

1. INTRODUCTION

The environment has suffered from industrial growth, especially in the textile sector, and water resources have been damaged [1,2, 3]. With over 10,000 tons released each year, the textile sector is the biggest user of dye [4,5]. Non-adsorbed dyes in wastewater cause cancer and other adverse health effects [6]. Dyes also deplete dissolved oxygen and obscure biological and photochemical processes, which is why they are bad for aquatic life [7,8]. Remediation of wastewater by dye removal is essential to environmental protection.

A number of methods are used to remove color from wastewater, including adsorption [9]. electrochemical treatment, biological treatment, membrane filtration, coagulation, photochemical degradation, and oxidation [4,10,11]. Wastewater color removal has been attempted using a number of techniques, but because of their limitations, none of them has been completely successful. Because synthetic dyes are light-stable, photochemical degradation is slowed down, coagulation decolorizes insoluble colors, and biological treatment procedures are hazardous, Economic exclusion is still a significant problem [12]. Of these, adsorption proved to be the most beneficial because of its low cost of operation, low susceptibility to contaminants, high efficiency, economic viability, and straightforward design [7,13].

Adsorption is a surface phenomenon that involves the adhesion of gases, liquids, and solids to the surface of the adsorbent [14]. It is a reliable and effective approach to handling industrial and domestic effluents [15]. An adsorbate is a substance that sticks to or concentrates at the surface, whereas an adsorbent is a substance on which adsorption is taking place [14,15,16]. Adsorption is primarily caused by the physisorption and chemisorption processes; physical sorption is the result of van der Waal forces of attraction, while chemisorption depends on the creation of a strong chemical bond between the adsorbent and the adsorbate [4].

In comparison to agricultural waste, other materials used as adsorbents are more costly, less accessible, and less renewable. One well-known adsorbent is activated carbon, which is offered because of its high adsorption capacity, broad surface area, and microporous structure [11]. Waste management and wastewater treatment are the two primary uses of low-cost adsorbents, which makes them a challenging sector [7].

Of all the sorbent materials suggested for eliminating contaminants from wastewater, activated carbon is the one that is most frequently utilized [17]. Because activated carbon adsorption is so good at removing different colors from wastewater, it's a great alternative to more costly treatment processes. Activated carbon does have several drawbacks, though, including price, issues with regeneration, lack of selectivity, and poor performance against vat and dispersed dyes [13]. For the majority of pollution management applications, it is therefore not justified to use carbon based on very expensive starting materials. Numerous workers have been forced to search for alternatives that are less costly [4].

Many researchers have employed agricultural waste materials for dye remediation of contaminated wastewater, including sawdust [18], raw maize cob, exhausted coffee ground powder [19], seed pods, black cumin, neem leaf, pineapple leaf, and pine tree leaves. Comparing agricultural wastes to other materials used as adsorbents, they are more affordable, more accessible, and more renewable [20].

Baobab**,** *Adansonia digitata* botanically, is a big, iconic tree indigenous to Africa, where it is found in many countries. It belongs to the Malvaceace family. Most scientists believed that the name “Baobab” originated from the Arabic name buhibab (fruit). Adansonia is derived in honor of the person who brought the seeds to Paris, Michel Adanson (1727–1806), while Digita was named due to its leaf shape, meaning hand-like. Baobab products serve as a source of food, fiber, and medicine in Africa, which makes them of great importance [21].

Cationic dyes are hazardous colorants used in coloring acrylic, wool, nylon, and silk, causing allergic dermatitis, skin rashes, mutagenesis, and cancer. They produce colorful cations in solution and are water-soluble. Azo and methane dyes contain cationic functionality. Basic dyes like crystal violet, methylene blue, basic blue, and basic red are visible, intense colors commonly used in textiles. Methylene blue exposure can cause health issues [22].

Methylene blue (MB) is a thiazine dye that is basic in nature. Broad uses for MB include coating paper stock, temporary hair color, coloring cottons and wools, and dyeing paper [23]. Methylene blue can have certain negative consequences, even if it is not particularly dangerous. Increased heart rate, vomiting, shock, the formation of Heinz bodies, cyanosis, jaundice, quadriplegia, and tissue necrosis are among the symptoms of acute exposure to

methylene blue in people [13,24].

In this work, we report the results of the adsorption of the cationic dye Methylene Blue (MB) over AD, HAD, and KAD adsorbents.

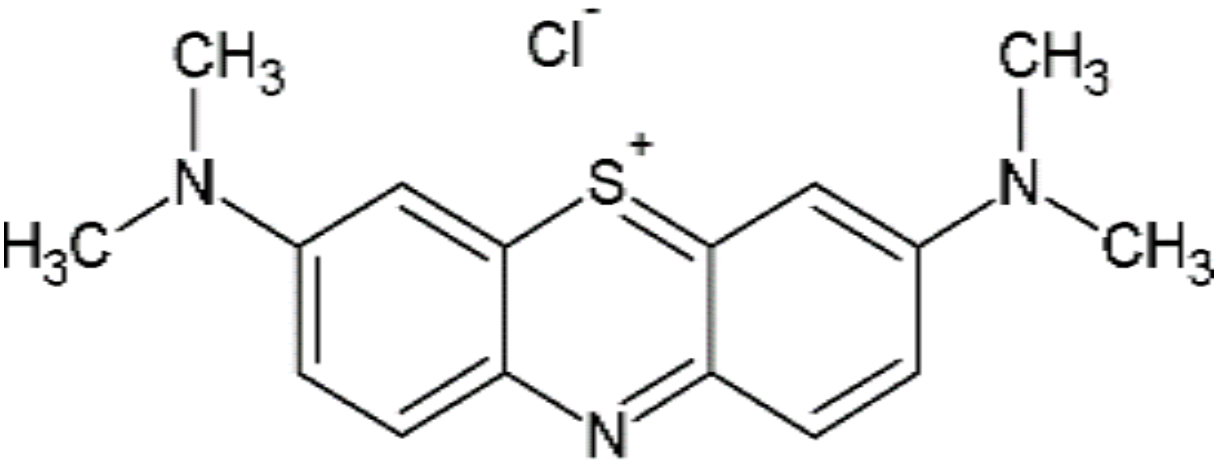

2. EXPERIMENTAL WORK

2.1 materials and methods

2.2. Adsorbate

The preparation of the methylene blue dye stock solution (1000 mg/L) involved dissolving 1 g of the dye in a 100 cm^3 beaker, transferring it to a 1000 cm^3 volumetric flask, and topping it up with distilled water. By appropriately diluting the stock solution with distilled water, the necessary experimental concentration (10, 30, 50, 70 & 100 mg/L) was created.

2.3. preparation of an adsorbent

The seed pod of Adansonia digitata was obtained from the Kurmi local market located in Kano State, Nigeria. To get rid of dust, debris, and other contaminants, the pod was thoroughly cleaned with water and then with distilled water. After being sun-dried for roughly 48 hours, the sample was again dried to a constant weight at 105 degrees Celsius in an oven. After being dried, the pod was mashed with a mortar and pestle and then sieved through a 0.2µm sieve to get a fine powder that was the biosorbent. After that, the biosorbent's sieved fine power was split into three parts. Without any additional processing, the first part was leveled as an AD adsorbent and kept in an airtight container. The second and the third portion of the sample were manually mixed for approximately 30 minutes, after impregnated with

85% concentrated H_3PO_4 and (KOH plus 100 cm^3 distilled water) respectively, in the ratio (2:1) wt/wt, dried at 110 ^oC in an electric oven for 24 hours and then carbonized at 600 ^oC separately using a muffle furnace [25]. After cooling down, the samples were leached with 0.1 M H_3PO_4 and 0.1 M KOH, and then they were carefully cleaned with distilled water until a pH of around 6.9 was reached [14]. The necessary activated carbon was produced during a 24-hour drying process at 110 ^oC in an oven.

2.4. Characterization

Fourier transform infrared (FTIR) and scanning electron microscopy (SEM) were used to characterize the adsorbents. Additionally, the bulk density, pH of the point zero charge, moisture content, and ash content were measured.

2.4.1. Determination of Percentage Yield

Product yield is a critical measure for determining the feasibility of an adsorbent from a specific precursor [26]. The percentage yield (%yield) of the manufactured activated carbon was determined by first weighing 100 g of the raw material (designated Mb), letting it cool, and then recalculating its weight using an electronic weighing scale as Ma, after the raw material was carbonized and activated at 600 °C.

Equation 2.1 was used to calculate the percentage yield of the precursor:

$$\%Yield = \frac{M_a}{M_b} \times 100 \quad (2.1)$$

Where M_a is the mass of the char and M_b is the initial mass of the sample [27].

2.4.2. Determination of Moisture Content

The moisture content was assessed to determine the hygroscopic characteristics of activated carbon. The moisture content was calculated on a dry basis. The empty, dry, and pristine crucible was weighed (W_1). One 2 g powdered sample of both treated and untreated biomass was added to the crucible after it had been weighed (W_2). After drying in an oven at 110 °C for 10 minutes, each sample was constantly weighed again until the weight stayed constant. The crucible holding the powdered sample that had dried was again placed in an oven at 110 °C. Weighing the crucible and sample once again was done (W_3). The moisture content was determined from the sample's weight loss using Equation 2.2

$$Moisture\ content = \frac{W_2 - W_3}{W_2 - W_1} \times 100 \quad (2.2)$$ [28,29]

Where W_1 is the mass of the empty crucible (g), W_2 is the mass of the crucible plus sample before drying (g), and W_3 is the mass of the crucible plus sample after drying (g).

2.4.3. Determination of Ash Content

To find the amount of ash, crucibles were heated to about 600 °C, cooled in a desiccator, and then weighed. Before being reweighed, each sample was placed into the crucibles, weighing 1.0 g. The crucibles containing the samples were then put in the furnace and heated to 600 °C for about an hour and thirty minutes. After that, they were cooled to room temperature (30 °C), and the samples were weighed once again. The ash content was calculated using Equation 2.3 [30]:

$$Ash\ content = \frac{ash\ weight}{Oven\ dry\ weight} \times 100 \quad (2.3)$$

2.4.4. Determination of Bulk Density

For the purpose of measuring bulk density, Sugumaran et al.'s (2012) procedures were slightly altered. Each powdered adsorbent sample was compressed to a 2 cm^3 mark in a glass cylinder (5 cm^3). Using Equation 3.6, the bulk density (g/cm3) was determined [31].

$$Bulk\ desity = \frac{mass\ of\ sample\ (dry)\ (g)}{Volume\ of\ packed\ dry\ sample\ (cm^3)} \quad (2.4)$$

All the experiments were carried out in triplicate, and the averages were presented.

2.4.5. pH of a point-zero charges

pH of Point of Zero Charge (pH_{pzc}): The pH at the point of zero charge (pH_{pzc}) is an important parameter in the study of adsorption phenomena, particularly when electrostatic forces are involved. pH_{pzc} is a relevant indicator of the chemical and electronic properties of the material used as an absorbent [33,34]. The salt addition method was used to measure this parameter in the following manner: solutions of 50 cm^3 of NaCl (0.1 M) were poured into a 250 cm^3 conical flask, and the initial pH (pH_i) was adjusted in each volume, ranging from 2 to 12, by adding 0.1 M solutions of KOH or HCl in drops. In each flask, 0.1 g of the adsorbent was added. The final pH (pH_f) of each solution was determined following filtration and 4 hours of

agitation at room temperature. Each solution was filtered and allowed to settle at room temperature for four hours before its final pH (pH_f) was measured. The pH_{pzc} values on a graph with $pH_f = f(pH_i)$ was obtained from the intersection of the pH curve with the first quadrant axis bisector The pH_{pzc} value was determined by graphing the point where the pH curve and the first quadrant axis bisector connect [33,34].

2.5. Batch adsorption experiment

To investigate the effects of adsorption settings, the experiment was conducted using a 250 cm^3 conical flask containing 100 cm^3 of the dye solution on an orbital incubator shaker set at room temperature and 200 rpm. 0.1 M HCl and 0.1 M KOH were used to raise the starting pH of the corresponding solutions to the appropriate levels (Yunusa and Ibrahim, 2020). In this experiment, a 100 cm^3 solution of the dye was mixed with 0.1–1.0 g of the produced adsorbent. Following agitation, the samples were filtered, and a UV spectrophotometer was used to determine the concentration. The ideal conditions were determined by adjusting the contact period (10–120 min), pH (2–12), dye concentration (10–100 mg/L), adsorbent dosage (0.1–1.0 g), and temperature (30^oC – 60^oC) during the optimization process. All procedures were run at room temperature, with the exception of the temperature effect, which was run at 30 to 60 degrees Celsius.

The adsorption capacity was determined using equation 2.5

$$q_e = \frac{C_i - C_e}{M} \times V \qquad (2.5)$$

Where V is the volume of the adsorbate solution, q_e is the dye uptake capacity (mg/g), M is the mass of the adsorbent in g, C_i is the initial dye concentration, and C_e is the dye concentration at equilibrium. The total efficiency in percent removal was calculated using equation 2.5

$$\% R = \frac{C_i - C_e}{C_i} \times 100 \qquad (2.6)$$

2.5.1. Determination of the effect of agitation time

With minor adjustments, the Yunusa & Ibrahim (2020) method was applied. A 100 cm^3 dye solution was placed in a 250 cm^3 Erlenmeyer flask along with the adsorbent (0.1 g). A

combination of 10, 20, 30, 40, 60, 90, and 120 minutes was the ideal agitation time. The adsorbent dose (0.1 g), temperature (30^{o}C), speed (200 rpm), and pH (the adsorbent's pH) were all held constant.

2.5.2. Determination of the initial concentration

A 100 cm^3 of the dye at different concentrations (10, 20, 30, 50, 70, and 100 mg/L) was mixed with 0.1 g of the adsorbent. At 200 rpm and 30 ^{o}C, the mixture was agitated using an incubator shaker to determine the ideal duration for each adsorbent. After that, the mixture was filtered, and the absorbance from the filtrate's UV analysis was used to determine the dye concentration [24].

2.5.3. Determination of the adsorbent dosage

With minor modifications, the method described by Yunusa & Ibrahim (2020) was used to add 0.1 g of the sample for every 100 cm^3 volume of adsorbate solution. The investigations were carried out at room temperature (30 °C) and 200 rpm for the ideal duration of each adsorbent. The samples were filtered and sent to a UV spectrophotometer for examination, where the concentration was found. The 0.1, 0.3, 0.6, 0.8, and 1.0 g adsorbent doses were shown to be optimal. The same process was applied to the remaining adsorbents.

2.5.4. Determination of the temperature

A minor modification was made to Yunusa and Ibrahim's (2020) approach in order to ascertain the impact of temperature. Whereby the optimal initial concentration of the adsorbent was increased to 100 cm^3 by adding 0.1 g of adsorbent. The mixture was stirred at the appropriate adsorbent agitation time, filtered, and the absorbance was measured with a UV-vis spectrophotometer. The calibration curve was used to determine the equilibrium concentration. All other parameters were held constant while the trials were conducted at 30, 40, 50, and 60 degrees Celsius.

2.5.5. Determination of the pH of the solution

Testing was done at pH values of 2, 4, 6, 8, 10, and 12. After each solution had been agitated for the ideal amount of time for each adsorbent and at the proper starting concentration, 0.1 g of treated and untreated samples were added individually for every 100 cm^3 of dye aqueous solution [24]. After filtering the mixture, the absorbance was measured to determine the

concentration [14].

2.6. Adsorption isotherms

It is impossible to overestimate the significance of the adsorption isotherm in describing the interactions between the adsorbent and the adsorbate and in giving an idea of the adsorption capacity. They are necessary in order to understand the adsorption mechanism. The Langmuir and Freundlich models provide the best description of the adsorption isotherm [4]. It is the connection between the species that can absorb an adsorbate and its amount [34].

2.6.1. Langmuir adsorption isotherm model

Separate from inter-individual interactions, this isotherm addresses external interactions of the adsorbent. The topic is adsorption in a monolayer. The linear form of the Langmuir model is as follows:

$$\frac{1}{q_e} = \frac{1}{q_{max}} + \left(\frac{1}{q_{max}K_L}\right)\frac{1}{C_e} \quad (2.7)\ [34,35]$$

K_L is the Langmuir constant ($dm^{-3}mol^{-1}$) and q_{max} = monolayer adsorption capacity (mgg^{-1}). This equation can be simply written as:

$$\frac{C_e}{q_e} = \frac{1}{q_{max}K_L} + \left(\frac{C_e}{q_{max}}\right) \quad (2.8)\ [34]$$

Generally speaking, adsorbate ionic strength, ionic medium, and pH all affect q_{max} and K_L. A straight line will be produced when we plot C_e (mgL-1)/q_e (mgg^{-1}) against C_e (mgL^{-1}). In order to determine whether the process is advantageous when $R_L > 1$ and linear for $R_L = 1$, in addition to irreversible for $R_L = 0$, R_L, or the separation factor parameter, was used. This is the formula for R_L;

$$R_L = \frac{1}{1+K_L C_i} \quad (2.9)$$

Where K_L = Langmuir adsorption equilibrium constant ($Lmol^{-1}$), C_i = initial dye concentration (mgL^{-1}). R_L can be determined from K_L and C_i [34].

2.6.2 Freundlich Adsorption Isotherm Model

Consider a heterogeneous adsorption surface with different adsorption energies and accessible sites that are dispersed unevenly. A non-linear empirical equation describing the multilayer

adsorption on the heterogeneous surface of the adsorbent with unevenly accessible active sites and inconsistent binding energy [34].

Freundlich suggested the following adsorption expression:

$$C_{ads} = K_F C^{1/n} \quad (2.10)$$

Integration of this equation gives the expression as:

$$\log C_{ads} = \log K_F + \frac{1}{n} (\log C_e) \quad (2.11)$$

Whereas C_{ads} indicates the concentration absorbed per unit mass of adsorbent ($molg^{-1}$), C_e indicates dye concentration at equilibrium ($molL^{-1}$). Adsorption strength and capacity are denoted by the Freundlich constants n and K_F, respectively. The value of n indicates the type of heterogeneous adsorbent that was used [37]. A larger amount of adsorption occurs when n is greater than one. Chinniagounder *et al*., (2011) and Nasar & Shakoor (2018) state that the value of n can range from 1 to 10 [35]. Good adsorption is indicated by a value of n between 2 and 10; moderate adsorption is indicated by a value of n between 1 and 2; and poor adsorption is indicated by a value of n less than 1 [35]. Equation 2.11 above can be resolved as follows:

$$\log q_e = K_F + \frac{1}{n} \log C_e \quad (2.12)\ [34]$$

Where: K_F = Freundlich constant, n is the slope, q_e (mg/g) is the amount of adsorbate adsorbed per gram of an adsorbent.

There is no limit to the amount of material that can be adsorbed using this adsorption isotherm, which employs multilayer adsorption [35].

2.6.3 Temkin Isotherm Model

The Temkin isotherm model's linear formulation, which considers the interactions between the adsorbent and adsorbate as follows:

$$q_e = \frac{R_T}{B_T} \ln K_T = \frac{R_T}{B_T} \ln C_e \quad (2.13)$$

Where R_T is the universal gas constant (8.314 $Jmol^{-1}K^{-1}$). The maximal binding energy and

the adsorption heat are represented by the Temkin isotherm constants, K_T (Lg^{-1}) and B_T ($kJmol^{-1}$), respectively. The quantity of K_T and B_T was determined using the linear plot of q_e vs. lnC_e.

2.7. Kinetics of Adsorption

To optimize various operating parameters for the biosorption process, kinetic studies are required. Numerous kinetic hypotheses have been used to explain the reaction's sequence. Fu *et al*., (2011) employed intraparticle diffusion, pseudo-first order, and pseudo-second order kinetic models, and was used to evaluate the MB dye's kinetics on biosorbents and biochars made from Adansonia digitata seed pods. Senthamarai *et al*., (2012) assessed the correlation coefficients (R^2) in order to evaluate the applicability of these kinetic models. When R^2 is high, the model may be applied to data most successfully [4].

2.7.1 Pseudo-first order model

The fundamental premise of the pseudo-first order kinetic model is that the dye concentration changes in a time-dependent manner in a proportional to power one manner. The integral form of the pseudo-first order model is usually expressed as follows:

$$\log(q_e - q_T) = \log q_e - k_1 . \frac{t}{2.303} \quad (2.14)\ [28]$$

where k_1 is the rate constant ($L\ min^{-1}$), t is the agitation period (min), and q_e and q_t are the biosorption capacities (mgg^{-1}) at equilibrium and time t, respectively. Tables 4.4a and 4.4b display the rate constants k_1, q_e-calculated, q_e-experimental, and R^2 values for the biosorption of MB employing biosorbents and biochars. Plotting log (q_e-q_t) against time in accordance with the Lagergren pseudo-first order model results in a straight line with a very low correlation value (R^2) [42].

2.7.2 Pseudo-second order kinetic model

The biosorption mechanism is explained across the contact time range by the pseudo-second-order kinetic model [32,33]. The different equation is shown as follows:

$$\frac{dq_t}{q_t} = k_2(q_e - q_t)^2 \quad (2.15)$$

Where K_2 ($g\ mg^{-1}\ min^{-1}$) is the second-order rate constant of biosorption process. By

integrating and applying boundary conditions t = 0 – t and q = 0 – q_t, the above equation can be written in linear form as follows:

$$\left(\frac{t}{q_t}\right) = \frac{1}{k_2 q_e^2} + \frac{t}{q_e} \quad (2.16)$$

Plotting t/q_t against t yields the values of the constants k_2 (g mg^{-1} h^{-1}) and q_e (mg g-1). The second order k_2, q_e-calculated, q_e-experimental, and R^2 values for the biosorption of methylene blue (MB) are shown in Tables 4.4a and 4.4b. The outcomes demonstrated a greater similarity between the experimental and computed q_e values. The correlation coefficient (R^2) values for native, processed, and immobilized biomasses are noticeably higher. Thus, the pseudo-second order kinetic model is more appropriate and efficient than the pseudo-first order kinetic model and shows the best fit to the kinetic data. These results are consistent with earlier reports [42].

2.7.3 Intraparticle diffusion model

There are several steps involved in the transfer of dye molecules from an aqueous solution to a biosorbent's surface. The biosorption mechanism can be adjusted using a single step or a combination of multiple steps. In the batch experiment setup, which involves fast and continuous stirring, the rate-determining or rate-controlling step may be film diffusion, intra-particle diffusion, or a mixture of both mechanisms. The intraparticle diffusion equation is written as follows:

$$q_t = K_{diff.} t^{1/2} + C_i \quad (2.17)$$

Where C_i (mg g^{-1} $min^{-1/2}$) is the intercept that describes the thickness of the boundary layer and K_{diff} (mg g^{-1} $min^{-1/2}$) is the rate constant of intraparticle diffusion. The intraparticle diffusion hypothesis predicts a linear curve for qt versus $t^{1/2}$. If intra-particle diffusion is involved in the biosorption reaction, then particle diffusion would be the controlling step if this line passed through the origin when the amount of solid adsorbed per unit mass of biosorbent (q_t) was plotted against the square root of time ($t^{1/2}$) [43].

The low value of the correlation coefficient (R^2) indicates that the primary factor impacting

the biosorption of MB onto biosorbents and biomasses is not intraparticle diffusion. We can deduce that both surface adsorption and intraparticle diffusion were active during the biosorption of MB dye onto biosorbents and biomass.

2.8. Thermodynamics of Adsorption

Certain state functions, such as change in Gibbs free energy (ΔG), entropy (ΔS), and enthalpy (ΔH), were utilized to calculate heat changes in a system or state of a system. These variables provided information about the characteristics of the adsorption process, such as whether it is endothermic or exothermic. All of these thermodynamic parameters can be computed using the following formulas [44]:

$$InK_c = -\frac{\Delta H}{RT} + \frac{\Delta S}{R} \quad (2.18)$$

Where ΔS is the entropy, ΔH is the enthalpy or total heat content of the system, T is the temperature, and K_c is the equilibrium constant.

$$K_C = \frac{C_{ads}}{C_e} \quad (2.19)$$

In which Kc, C_{ads}, and C_e stand for the equilibrium constant, the equilibrium concentration of dye remaining in solution (mol/L), and the quantity of dye adsorbed on the adsorbent (mol/L) at equilibrium, respectively. The adsorption process is exothermic if the Gibbs free energy change is negative. The relationship between enthalpy, entropy, and Gibbs free energy change is as follows [34]:

$$\Delta G = \Delta H - T\Delta S \quad (2.20)$$

3. RESULT AND DISCUSSION

3.1. Characterization of the Adsorbent and Adsorption Test

3.1.1 Percentage Yield

In summary, the base-activated carbon (KAD) yielded 18%, whereas the acid-activated biomass (HAD) demonstrated a greater yield of 29%. This is because a higher yield of char was produced by the enhanced conversion of aliphatic to aromatic molecules caused by H_3PO_4 activation [45].

3.1.2 Moisture Content, Ash Content, and Bulk Density

Table 3.1. Moisture Content, Ash Content and Bulk Densities of the Adsorbents

S/N	Adsorbent	Moisture Content (%)	Ash Content (%)	Bulk Density (g/cm^3)
1	AD	2.48	5.2	0.26
2	HAD	6.31	27	0.24
3	KAD	10.56	19	0.2

The adsorption capability decreases as the moisture content increases. Due to the fact that the water (H_2O) molecule will compete with the adsorbent for binding to or adhering to its active sites, Furthermore, the adsorption capability decreases with increasing ash content. This is because the ash's mineral content will cover or obstruct the adsorbent's porous structure, which will reduce the amount of color that is absorbed. The bigger the bulk density and, correspondingly, the higher the adsorption capacity, the finer the particle size. Consequently, based on Table 3.2's results, untreated biomasses (AD) will have a higher adsorption capacity because of their higher bulk density, minimal moisture content, and ash content.

3.1.3. Effect of Point of Zero Charge (pH_{pzc})

The sites of zero charge for AD, HAD, and KAD were found to be 6.6, 6.8, and 7.0, respectively, using the solid addition method, as seen in Figure 3.1. At pH levels higher than pH_{pzc}, the biomass has a negative surface charge. Otherwise, if the solution's pH is less than pH_{pzc}, the material's surface has a positive charge. Surface charge is zero at pH_{pzc}, which indicates that net negative charges and total positive charges equal a neutral surface [46].

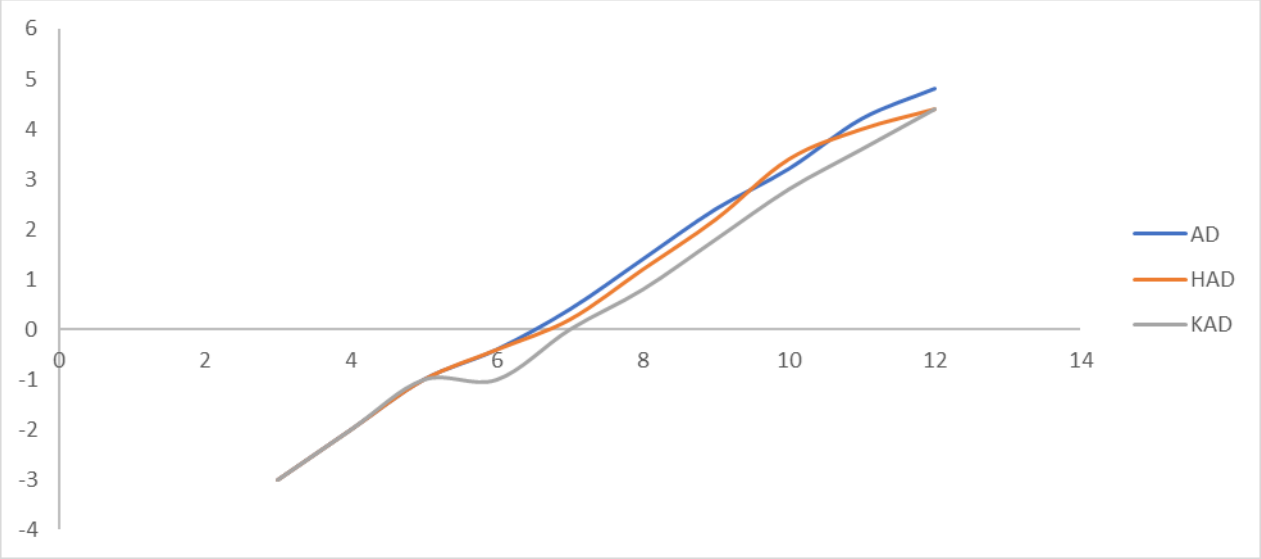

Fig.3.1. pH of point zero charge of AD, HAD and KAD adsorbents

3.1.4 Fourier Transform Infrared Spectroscopy Analysis (FTIR)

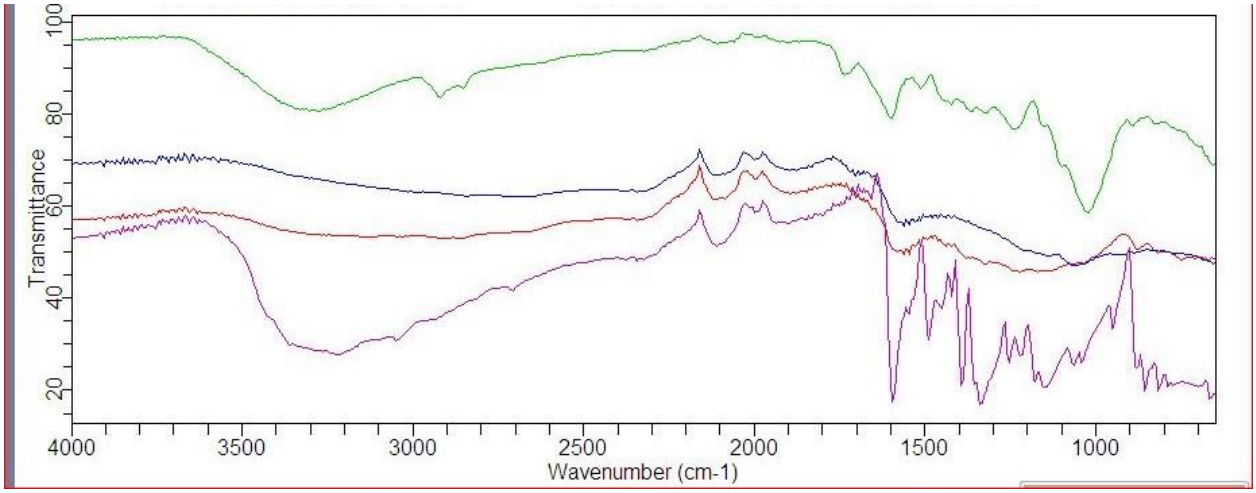

AD _____ HAD-before Adsorption_____ HAD-after Adsorption_____ MB_____

Fig.4.3. Fourier Transform Infrared Spectroscopy (FTIR) spectra of MB Adsorption onto AD and HAD

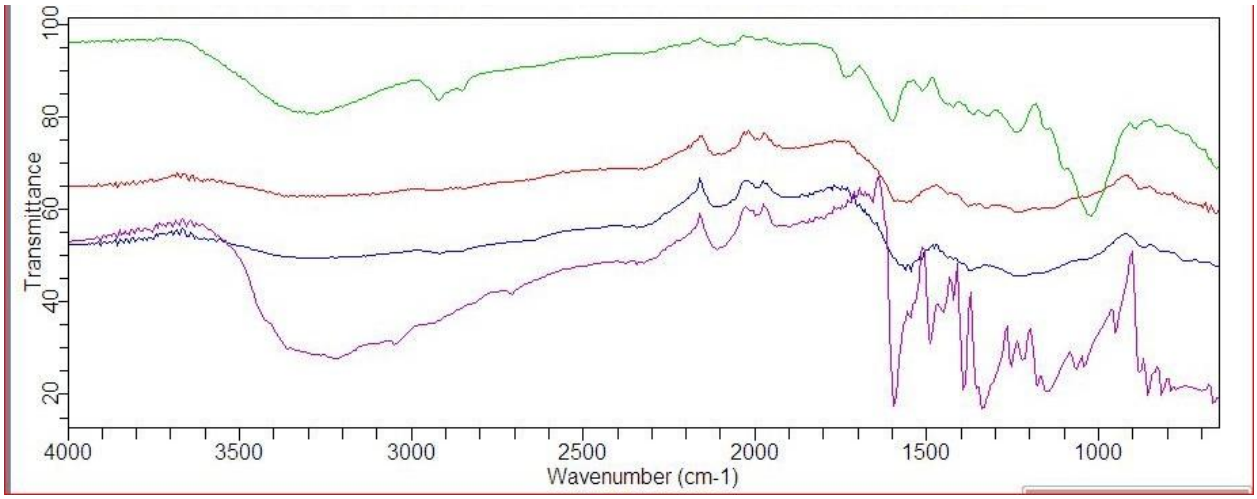

AD _____ KAD-before Adsorption_____ KAD-after Adsorption_____ MB_____

Fig.4.4. Fourier Transform Infrared spectroscopy (FTIR) Spectra of MB adsorption onto AD and KAD

The AD biomass before and after activation (KAD and HAD), followed by the adsorption of methylene blue, revealed significant changes in the infrared absorption bands, indicating alterations in the functional groups present on the biomass surface. The broad band observed in the range of 3100 to 3500 cm^{-1} is commonly attributed to O-H stretching vibrations in hydroxyl groups [14] and N-H stretching vibrations in amine groups, i.e., the width of the band indicates a H-bond [46]. A similar result was reported by Üner *et al*. (2017). Remarkably, this band was no longer detectable after the acid and base activation and methylene blue adsorption processes. This could be indicative of a reduction in hydroxyl and amine groups, possibly due to the modification induced by acid treatment and the subsequent adsorption of methylene blue.

The double band around 2900 cm^{-1}, which typically corresponds to C-H stretching vibrations in aliphatic hydrocarbon chains, was conspicuously absent in the post-treatment spectra [8]. This absence suggests a depletion of aliphatic hydrocarbons due to the acid activation process. The weak absorption band at around 2100 cm^{-1}, indicative of C≡N triple bond stretching vibrations, exhibited an increased intensity in the post-treatment spectra. This suggests the formation or enrichment of nitrile groups, possibly facilitated by the acid activation process

and enhanced by the adsorption of methylene blue. The sharp band with medium intensity observed around 1600 cm^{-1} is typically associated with C=C stretching vibrations in aromatic compounds [46] and C=O stretching vibrations. In the post-treatment spectra, a reduction in the intensity of this band was evident, implying an increase in the aromatic compounds, potentially affected by both the acid activation and the adsorption of methylene blue.

The sharp and medium band at around 1000 cm^{-1}, which is often attributed to C-O stretching vibrations of cellulose, hemicellulose, and lignin in ether or alcohol functional groups [14], exhibited decreased intensity in HAD and disappeared in HAD and KAD (elongation vibrations confirm the presence of carboxyl/alcohol/ether/ester functional groups in the molecular composition of the bio-absorbent) [46]. This suggests a reduction in ether or alcohol groups, possibly due to the modifications induced by acid activation and the subsequent adsorption of methylene blue.

For methylene blue, a broad, strong band was observed at 3100–3200 cm^{-1}, indicating O-H stretching vibration, and a broad, medium band at 2100 cm^{-1}, indicative of C≡N triple bond stretching vibrations. There is also a sharp band around 1600 cm^{-1}, which is typically associated with C=C stretching vibrations in aromatic compounds [46]. Similar findings were also reported by Üner *et al*. (2017). They disappeared due to activation and adsorption processes. Also, a strong, sharp band was observed at 1300–1400 cm^{-1}, which is attributed to C-H bending of the methyl group.

3.1.5. Scanning Electron Microscope (SEM)

The morphological characteristics of the used adsorbents were assessed before and after the adsorption of Methylene blue dyes, and the obtained results are displayed in the following figures:

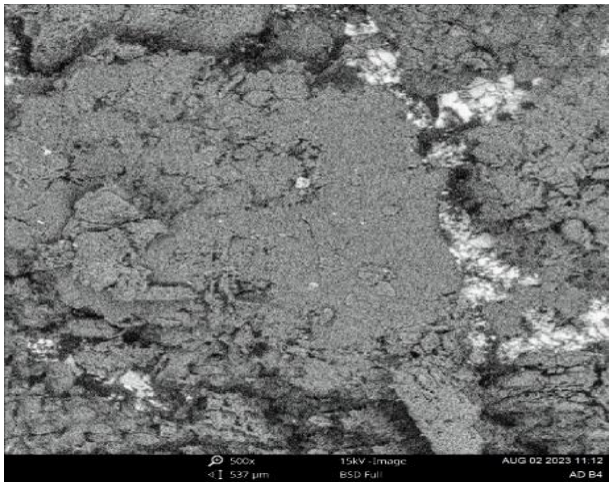
500x 15kV - Image AUG 02 2023 11:12
537 µm BSD Full AD B4

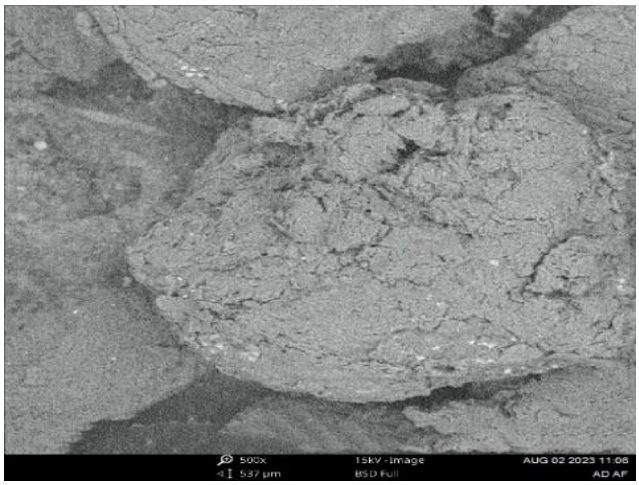
500x 15kV - Image AUG 02 2023 11:08
537 µm BSD Full AD AF

c

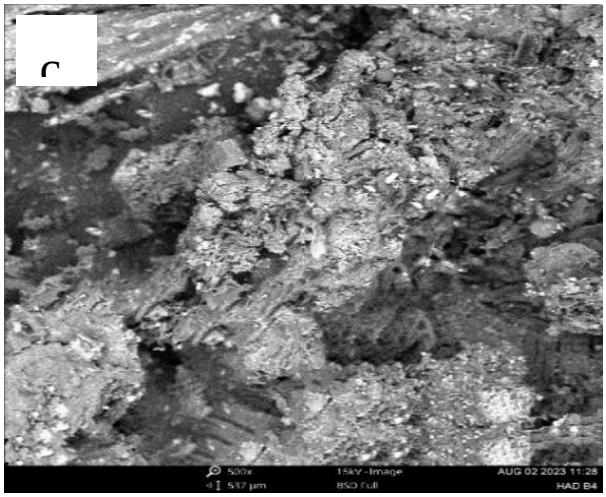
500x 15kV - Image AUG 02 2023 11:28
537 µm BSD Full HAD B4

d.

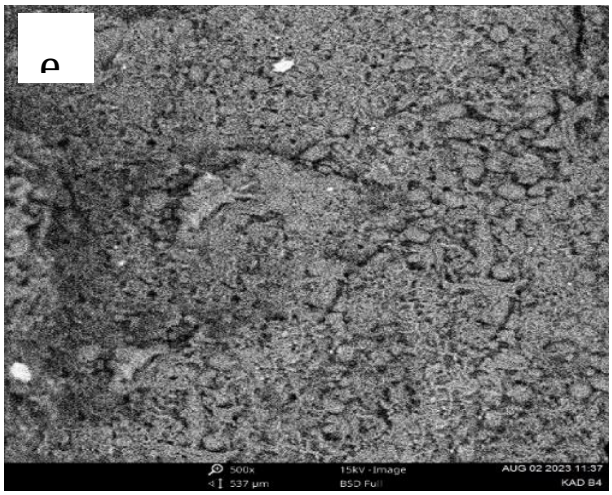

f.

Plate 3.1. SEM micrographs (×500) of (a) AD-before, (b) AD-after, (c) HAD-before, (d) HAD-after, (e) KAD-before & (f) KAD-after adsorption

The SEM images before and after adsorption show that adsorption has occurred by showing alterations in the micrographs.

The surface morphology and pore structure of the AD, KAD, and HAD adsorbents before and

after adsorption were investigated using scanning electron microscopy (SEM), and the results are presented in Plate 3.1. The results revealed a significant enhancement in the surface porosity and texture of AD after activation and carbonization, and the SEM images of the adsorbed material provided insights into the extent of pore filling and dye adsorption [47]. The micrographs displayed an intricate network of pores and ridges on the surfaces of KAD and HAD, indicative of the increased porosity and texture achieved through the activation processes [8]. The surfaces were observed to be significantly rougher and more irregular compared to the untreated biomass feedstock, AD. Upon adsorption of methylene blue dye, the SEM images displayed the distribution of dye molecules on the HAD material's surface. The dye molecules appeared as clusters, covering the porous structure. This observation suggested effective dye adsorption, wherein the dye molecules were able to interact with the surface through electrostatic forces and π-π stacking interactions. The degree of dye covering as shown in the results reflects the materials' adsorption capacity.

3.2 Effect of Operational Conditions

3.2.1. Effect of Agitation Time

The adsorption rate must be considered in an appropriate adsorption system. The adsorption process is affected by contact time, as shown in Figure 4.4 below.

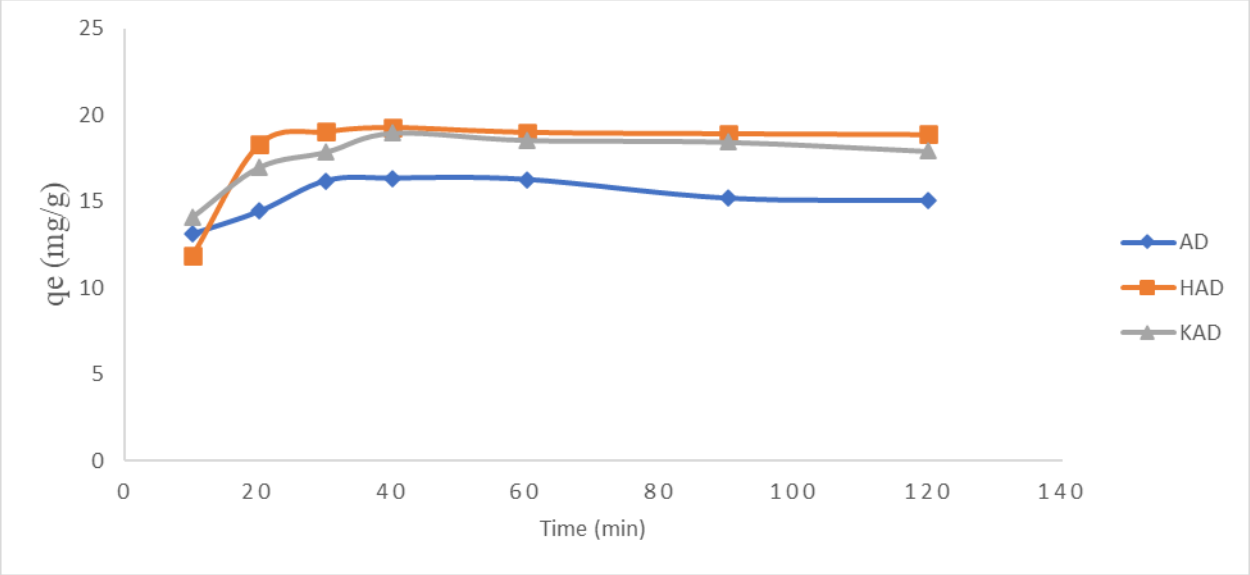

Fig.3.4. Effect of agitation time of MB adsorption onto AD, HAD, and KAD

Figure 3.4 illustrates how the adsorption capacity of each adsorbate increases rapidly in the

beginning, reaching 19.97 mg/g for both HAD and KAD after 40 minutes of agitation time. After that, the adsorption capacity gradually decreased as the agitation time increased and eventually became nearly constant. After attaining equilibrium, further adsorption under the employed conditions was insignificant as a function of contact time. A large concentration difference between the bulk liquid and the solid surface adsorbent is what causes the early, rapid absorption. The low number of empty sites was the reason for the slight increase in adsorption capacity at later phases, which was matched by a slow increase [42,48]. The residual empty spaces are gradually filled by adsorbate molecules due to the repulsive interactions between the liquid and solid phases [14]. Thus, for additional adsorption research, an ideal duration of 40 minutes was [48]. The percentage removal rises as the agitation time increases, and dye desorption begins as the contact time climbs even higher. This is due to the fact that dye molecules are only loosely bonded to the adsorbent surface during saturation [35]. Stated differently, the adsorbent's active sites were impregnated with the dye molecules at the saturation point [49].

3.2.2. Effect of Initial Concentration

The adsorption process, which can significantly induce the solute molecules to overcome mass transfer resistance between the liquid and solid phases, is known to be significantly influenced by the initial dye concentration.

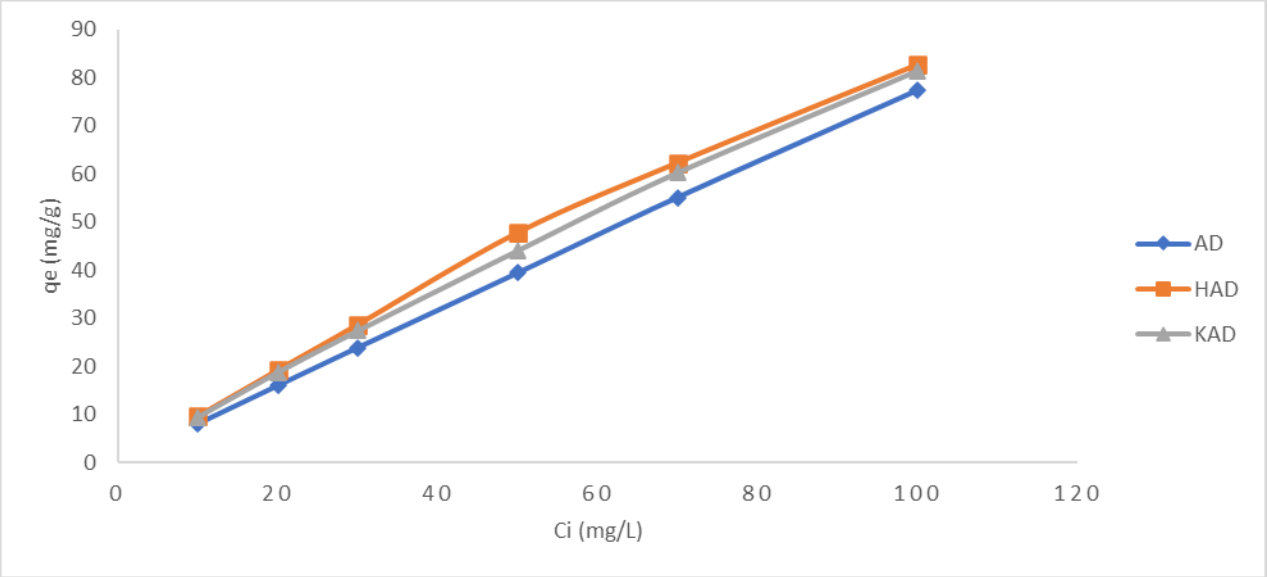

Fig.3.5. Effect of initial concentration of MB adsorption onto AD, HAD and KAD

The effect of varying starting dye concentrations on the adsorption capacity of the adsorbate, MB, is demonstrated in Figure 3.5. Additionally, using an initial dye concentration of 100 mg/L, it demonstrated the greatest dye uptake of 81.46 mg/g for all three adsorbents (AD, HAD, and KAD). With an increase in starting concentration from 10 mg/L to 20 mg/L, an increase in adsorption capacity was observed for the previously described adsorbents from 9.44 to 18.78 mg/g, respectively. The large driving force for mass transfer at a high starting dye concentration could be the reason for this [50].

3.2.3. Effect of Adsorbent Dosage

The impact of 0.1–1.0 g of biochar on the adsorption capacity of 50 mg/L concentrations of cationic MB at room temperature is shown in Figure 3.6. This illustrates the exceptional sorption capacity of biochar for the removal of dye-contaminated water.

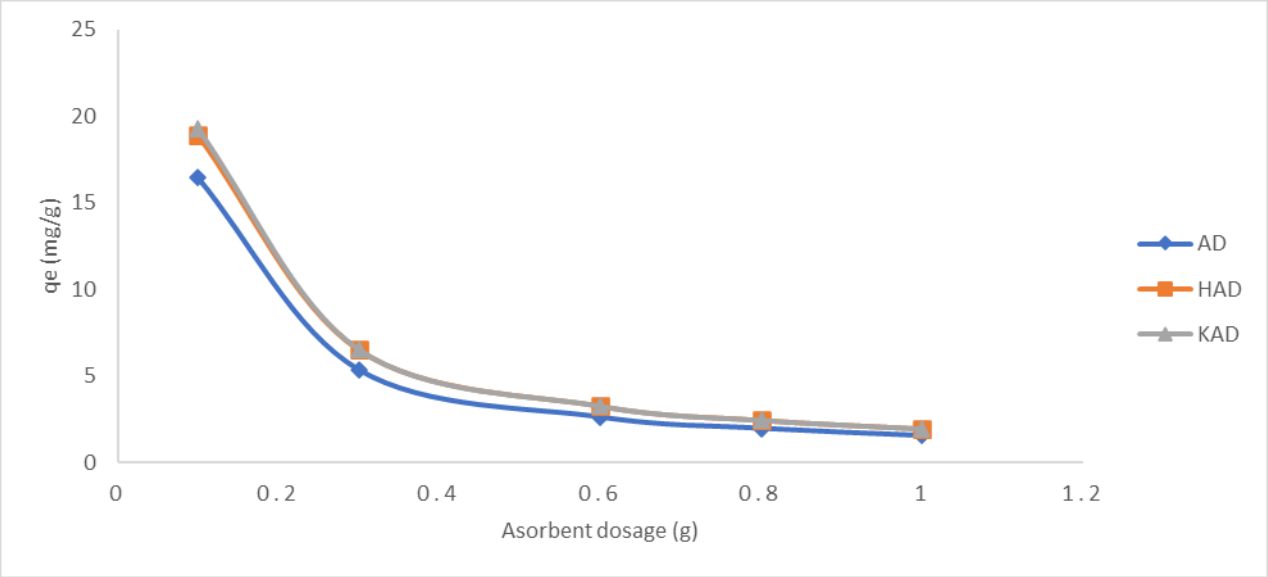

Fig.3.6. Effect of adsorbent Dosage of MB adsorption onto AD, HAD and KAD

As the dosage of biochar increased, the adsorption capability of all three hues considerably decreased (Figure 3.6). However, beyond a certain dosage, it stopped decreasing with more biochar. The maximal adsorption capabilities of the dye were found to be 16.45 to 5.35 mg/g on AD and 19.26 to 6.54 mg/g on both HAD and KAD adsorbents using 0.1 to 0.3 g of the adsorbents. At the lowest adsorbent dosage of 0.1 g, the highest adsorption capabilities of MB dye onto the aforementioned adsorbents were found to be 16.45 mg/g for AD and 19.26 mg/g

for both HAD and KAD. This indicates the exceptional sorption capacity of biochar for the removal of dye-contaminated water. Furthermore, an increase in doses was accompanied by a drop in q_e at biochar dose values greater than 0.4 g, after which q_e became nearly constant. The increased adsorption of dyes at lower dosages of biochar can be explained by an increase in the ratio of dye to adsorbent molecules, which enhances the dyes' sorption ability. Reduced adsorption capability at higher dosages may be the result of binding site overlap, insufficient dye molecule availability for unoccupied active sites, or both when biochar dosage is increased at fixed dye concentrations [51]. The results showed that when the dosage of the adsorbent is increased, the MB dye's ability to bind to AD, HAD, and KAD adsorbents decreases. The achievement of equilibrium resulted in a decrease in the adsorption capacity, suggesting that any additional addition caused desorption [35].

3.2.4. Effect of Temperature

The effect of temperature on the adsorption rate of MB dye onto AD, HAD, and KAD adsorbents was investigated, as inferred from Figure 3.7, at 303, 313, 323, and 333K.

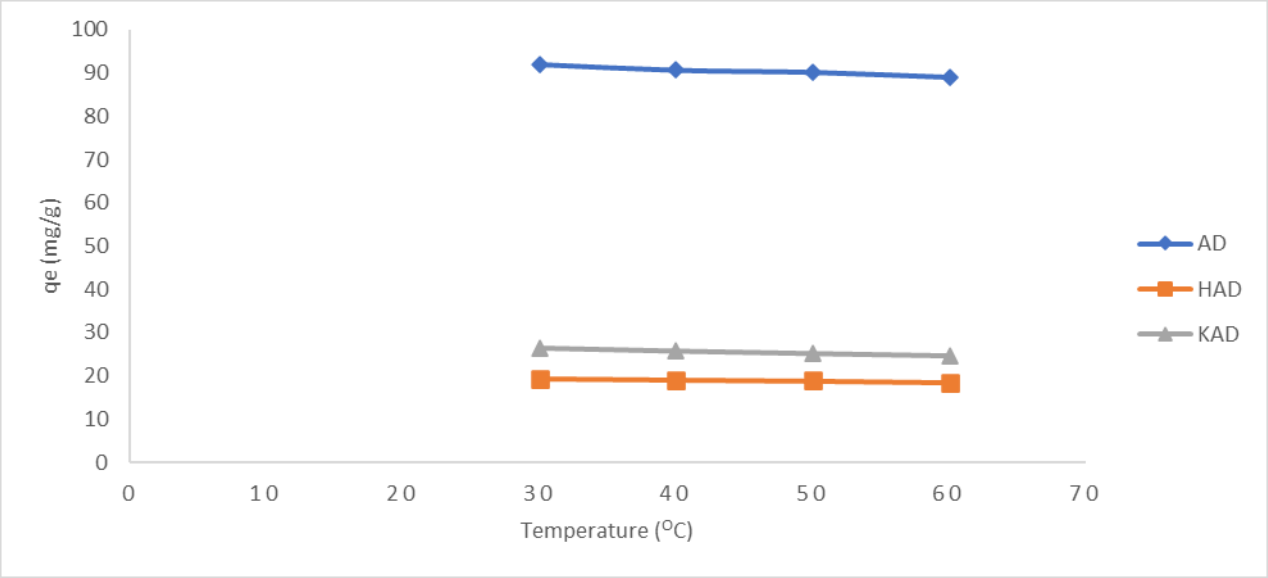

Fig.3.7. Effect of adsorbent Temperature of MB adsorption onto AD, HAD and KAD

Raising the temperature is also known to accelerate the rate of diffusion of the adsorbate molecules past the outer boundary layer and inside the pores of the adsorbent particle due to the decrease in solution viscosity that occurs with an increase in temperature. With a rise in temperature (303 to 333 K), the adsorption capacity of AD, HAD, and KAD adsorbents fell

from 92.06 to 88.97, 19.34 to 18.53, and 26.38 to 24.67 mg/g respectively. This indicates that the reaction is exothermic and implies physisorption. This could be because when temperatures rise, dye molecules become more mobile. Additionally, an increasing number of molecules may accumulate sufficient energy to interact with active sites [24]. The maximum amount of dye removed occurs at 30 ^{o}C, the lowest temperature, and then the amount gradually drops from there. This could be because molecules that are adsorbed at high temperatures have more kinetic energy. Because dye prefers to be soluble in the solvent rather than adsorb on the adsorbent surface, adsorbate-solvent interactions reduce both the adsorption capacity and the percentage of dye removal. As a result, the process's exothermic nature was discovered [35]. Rising temperatures may also have an internal swelling effect. Larger dyes have a greater ability to permeate the internal structure of the adsorbent [24].

It was discovered that when temperatures increased, the proportion of elimination decreased. This may be because physical adsorption at higher temperatures increases entropy, which reduces the forces holding the adsorbed species and the adsorbent's active sites together. Desorption into the aqueous solution may therefore cause the fraction of adsorbed molecules to drop. The achievement of equilibrium resulted in a decrease in the adsorption capacity, suggesting that any further increase would cause desorption [52].

3.2.5. Effect of pH

The pH of the dye solution has a major impact on the entire adsorption process, specifically the adsorption capacity. The effect of pH on the adsorption of MB at equilibrium for the three absorbents (AD, HAD, and KAD) is shown in Figure 3.8.

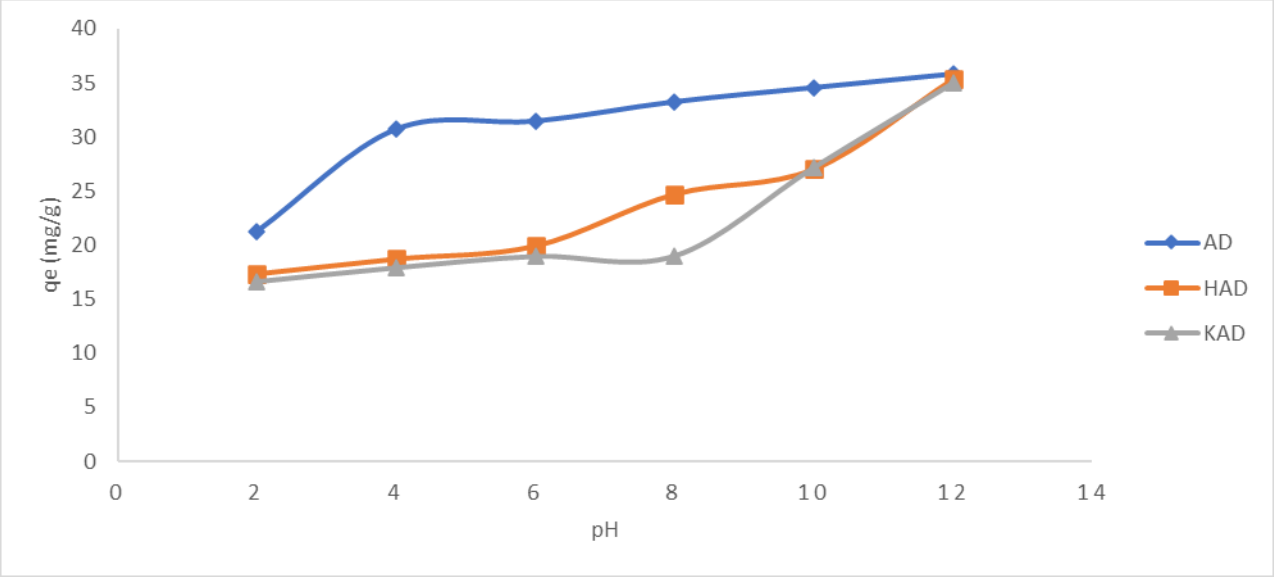

Fig.3.8. Effect of pH of MB adsorption onto AD, HAD and KAD

It was found that as pH increased, the q_e increased. The lower adsorption at acidic pH was probably caused by the extra H^+ ions competing with the dye cations for adsorption sites [24]. In contrast, the excess OH^- in the basic medium causes the adsorbent's surface to become negatively charged, which causes an electrostatic attraction between the negatively charged adsorbent surface and the cationic dye, improving both dyes' adsorption at a basic pH [14].

In this regard, it is noteworthy that the significant effect of pH on adsorption can be more effectively explained by the point of zero charge (pH_{zpc}), an adsorbent characteristic. The pH_{zpc} of the activated carbons and biosorbents for the two adsorbents were found to be between 6.6, 6.8, and 7.0 for AD, HAD, and KAD, respectively (Figures 3.1). The adsorbents are therefore more likely to readily adsorb any cationic dye at pH levels higher than these values when the pH_{zpc} values for AD, HAD, and KAD are greater than 6.6, 6.8, and 7.0, respectively. The higher elimination at basic pH ranges could be explained by the cationic nature of MB dye. Consequently, the observed higher adsorption in basic fluids is most likely due to the strong electrostatic contact between the positively charged cations and the negatively charged adsorbent. Furthermore, a medium with a pH higher than 6.6 is optimal for the adsorption of anionic dyes, as shown by the pH of the adsorbent's point zero charge [14].

3.3. Adsorption Isotherms

The relationship between a chemical's concentration in the equilibrium solution and the

amount adsorbed at a constant temperature is found using adsorption isotherms. Three isotherm factors were taken into account in this study. Freundlich, Temkin, and Langmuir isotherms.

3.3.1. Langmuir Isotherm

Equations 2.7 or 2.8 provide a straight line with an intercept of $1/Kq_{max}$ and a slope of $1/q_{max}$ when plotted against C_e. The separation factor, defined in many systems using equation 2.9, is a term used to characterize the fundamental characteristics of the Langmuir isotherm. It is also referred to as the equilibrium constant (R_L).

3.3.2. Freundlich Isotherm

Plotting log q_e and log C_e using equation 2.12 results in a straight line with an intercept of (K_F) and a slope of (1/n). This is a standard method for representing experimental data to facilitate the computation of the constants (K_F) and (n) and the assessment of the success of material removal from solution.

3.3.3 Temkin Isotherm

The solution to the equation 2.13 produced a plot of q_e versus In C_e, from which the equilibrium binding constants (L/mg) corresponding to maximal binding energy could be calculated.

Table 3.2. Isotherm Parameters for Adsorption of MB dye onto AD, HAD and KAD adsorbents

Isotherm	Parameters	AD	HAD	KAD
Langmuir	q_{max}	416.67	100.00	813.01
	K_L	0.01	0.31	0.02
	R_L	0.83	0.14	0.68
	R^2	1.0000	0.9971	0.9950
Freundlich	N	1.07	1.89	1.66
	1/n	0.93	0.53	0.60
	K_F	1.90	3.82	3.25
	R^2	0.9995	0.9254	0.9909
Temkin	B_T(J/mol)	27.84	18.85	20.05

K_T(L/mg)	0.50	4.19	2.12
R^2	0.9173	0.9799	0.9488

Table 3.2 presents the outcomes of the experiment. As a result of their close proximity to unity, the maximum R^2 values for MB dye were determined to be 1.0000, 0.9971, and 0.9950 for AD, HAD, and KAD, respectively. These values best match the Langmuir adsorption isotherm. Therefore, MB onto HAD shown the best fit with Langmuir > Temkin > Freundlich, whereas MB onto AD and KAD correlates best with Langmuir > Freundlich > Temkin.

The process's favorable or unfavorable status was ascertained using the separation factor parameter (R_L) for the Langmuir isotherm, which is provided in Table 3.2. According to Sajid et al. (2022), the process is irreversible for $R_L = 0$ and linear for $R_L = 1$, and unfavorable when $R_L > 1$. It is also advantageous when $0 < R_L < 1$. Since the R_L values are both greater than zero and less than one, all of the processes are advantageous for Langmuir.

The Freundlich constants K_F and n, respectively, stand for adsorption strength and capacity. According to Sajid et al. (2022), adsorption occurs more frequently when n is larger than unity. n denotes the heterogeneous surface of the adsorbent and can range from 1 to 10. Good adsorption is indicated by a value of n between 2 and 10; moderate adsorption is indicated by a value of n between 1 and 2; and poor adsorption is indicated by a value of n less than 1. The current approach obeys the Freundlich isotherm condition because all values of n were found to be more than one (that is, for MB onto both AD, HAD, and KAD, the value of n is between 1 and 2, suggesting moderate adsorption) [35].

3.4. Kinetic Studies

To determine the optimal adsorption exposure period, reaction kinetics research is crucial in addition to understanding the adsorption mechanism. To investigate the adsorption mechanism, a number of kinetic models have been used, including intra-particle diffusion kinetic models, pseudo-first-order, and pseudo-second-order models. While the intra-particle diffusion model helps to understand the adsorption kinetics, pseudo-first- and pseudo-second-order models are useful for the rate-determining stages [35].

Generally, three sequential steps are used to construct diffusion models: (1) solute diffusion

inside the pores of the adsorbent, also known as "intra-particle diffusion"; (2) solute diffusion across the liquid film surrounding the adsorbent material, also known as "film diffusion"; and (3) adsorption of adsorbate on the active site of the adsorbent. Reaction models generated from chemical reaction kinetics, however, rely on the full adsorption process without accounting for the previously described stages [14].

Table 3.3. Kinetic Parameters for Adsorption of MB dye onto AD, HAD and KAD adsorbents

Kinetics	Parameters	AD	HAD	KAD
Pseudo first	q_e (mg/g)	1.08	1.28	1.40
	k^1	0.03	0.02	0.05
	R^2	0.5464	0.4883	0.6145
2nd-Pseudo	q_e (mg/g)	16.67	19.96	19.53
	k^2	0.03	0.02	0.02
	R^2	0.9995	0.9976	0.9994
	$q_{e.exp}$(mg/g)	16.40	19.50	19.00
Intra-particle	K_{diff}	0.35	0.64	0.52
	R^2	0.5787	0.4192	0.6216

The pseudo-second-order rate constant can be found using the graph of t/qt against t. The kinetic data obtained in this investigation were fitted using the pseudo-first-order, pseudo-second-order, and intra-particle diffusion models in Table 3.3, which also contains the relevant values for these models. By comparing the correlation coefficient values, it is possible to deduce that the pseudo-second-order model provides a reasonably good match to the kinetic data of each adsorbate. The kinetic data could not be satisfactorily explained by either the intra-particle diffusion or the pseudo-first-order model; however, the pseudo-second-order $q_{e.cal}$ (for MB 16.67, 19.96, and 19.53 mg/g onto AD, HAD, and KAD adsorbents, respectively) did, as demonstrated by a comparison with their experimental adsorption capacities ($q_{e.exp}$) of 16.40, 19.50, and 19.00 mg/g, which are very close to each other (Table 3.2). As a result, the pseudo-second-order model fits the data collected better when it comes to describing adsorption systems. According to a number of studies, the

pseudo-second-order model faithfully describes how metals and dyes are adsorbed from aqueous solutions [14]. The pseudo-second-order model was determined to be suitable for the adsorption process based on its correlation coefficients, which are 1.9995, 0.9976, and 0.9994 for AD, HAD, and KAD adsorbents, respectively. These values are all close to unity.

3.5. Thermodynamic Studies

The thermodynamic parameters play a major role in the assessment of the nature and properties of the adsorption process in terms of their physicochemical aspects. Adsorption enthalpy, entropy, and Gibbs free energy all contain basic information about adsorption. ΔG, or Gibbs free energy change, indicates if the adsorption process is spontaneous or not. Enthalpy change (ΔH) indicates the thermal character of the process, indicating whether it is exothermic or endothermic, whereas entropy change (ΔS) measures the degree of disorder among the molecules that make up the adsorbent and the adsorbate [14]. In the case where ΔG is negative (smaller than zero), no external energy is needed for the adsorption process to occur. If ΔG > 0 (positive) is present, it means that the reaction mechanism requires a supporting force, often heat energy, and that the sorption does not happen spontaneously. In general, it is preferable for ΔG to be spontaneous (a negative number) for the best adsorption process.

Table 3.4. Thermodynamic Parameters of MB dye adsorption onto AD, HAD and KAD adsorbents

Adsorbent	ΔH(kJ/mol)	ΔS(kJ/mol/K)	ΔG(kJ/mol)			
			30°C	40°C	50°C	60°C
AD	-9.64	-0.0116	-6.13	-6.02	-5.9	-5.79
HAD	-23.11	-0.0483	-8.47	-7.99	-7.51	-7.02
KAD	-12.61	-0.0252	-4.97	-4.97	-4.46	-4.21

Table 3.4 provides evidence that the adsorption process as a whole yield a negative ΔG, indicating that the adsorption is spontaneous and occurs without the need for external energy [53]. It's evident that ΔH is completely negative, pointing to an exothermic process where temperature increases cause the adsorption capacity to decrease [33]. The quantity of ΔH can

be used to determine the type of adsorption, according to similar behavior documented in another paper by Akter *et al*., (2021). The heat produced by physical adsorption is 2.1-20.9 $kJmol^{-1}$, the same as that produced by condensation, whereas the heat produced by chemisorption is frequently 80–200 $kJmol^{-1}$. According to Akter et al. (2021), the range of ΔH values indicates that MB dye adsorption onto AD, HAD, and KAD is physical adsorption.

A positive ΔS value suggests that the process is dissociative, that the adsorbent and adsorbate are attracted to each other, and that the degree of freedom and randomness at the solid-liquid interface are increasing [53]. On the other hand, the positive values of ΔS for the MB onto AD adsorbent indicated an increase in the randomness of the adsorbate's molecules on the solid surface of the adsorbent than in the aqueous solution. The results show that unpredictability decreases near the solid-solution interface, or they indicate a decrease in the randomness of the adsorbates' molecules on the solid surface of the adsorbents compared to in the solution [33]. These negative values of ΔS were obtained for MB adsorption onto HAD and KAD adsorbents.

4. CONCLUSIONS

It was discovered that Baobab (Adansonia digitata) seed pods, a very accessible and inexpensive agricultural waste, worked incredibly well to remove MB from synthetic wastewater. The Langmuir, Freundlich, and Temkin isotherm models were utilized to examine the equilibrium data. Using an adsorbate concentration of 100 mg/L, the maximum adsorption capabilities of MB were determined to be 92.06 mg/g for AD and 81.46 mg/g for both HAD and KAD. For all three adsorbents, equilibrium values fit the Langmuir isotherm extremely well. With computed adsorption capacity (qe) values that are similar to experimental adsorption capacity (qe.exp) values, the adsorption processes were shown to fit the pseudo-second-order kinetic model.

5. ACKNOWLEDGEMENTS

The authors wish to acknowledge the support of the chief laboratory technicians, chemistry and biochemistry departments as well and the entire staff of chemistry department, Bayero

University Kano, Nigeria for the success of this work.

It was discovered that Baobab (Adansonia digitata) seed pods, a very accessible and inexpensive agricultural waste, worked incredibly well to remove MB from synthetic wastewater. The Langmuir, Freundlich, and Temkin isotherm models were utilized to examine the equilibrium data. Using an adsorbate concentration of 100 mg/L, the maximum adsorption capabilities of MB were determined to be 92.06 mg/g for AD and 81.46 mg/g for both HAD and KAD. For all three adsorbents, equilibrium values fit the Langmuir isotherm extremely well. With computed adsorption capacity (q_e) values that are similar to experimental adsorption capacity ($qe._{exp}$) values, the adsorption processes were shown to fit the pseudo-second-order kinetic model.

6. REFERENCES

[1] Charumathi, D., and Das, N. (2012). Packed bed column studies for the removal of synthetic dyes from textile wastewater using immobilised dead C. tropicalis, *Desalination*, 285, 22–30.

[2] Dargo, H., Gabbiye, N., and Ayalew, A. (2014). Removal of Methylene Blue Dye from Textile Wastewater Using Activated Carbon Prepared from Rice Husk. *International Journal of Innovation and Scientific Research 9*(2), 317–325.

[3] Le, T. T., Murugesan, K., Lee, C-S., Vu, C. H., Chang, Y.S., and Jeon, J-R. (2016). Degradation of synthetic pollutants in real wastewater using laccase encapsulated in core–shell magnetic copper alginate beads, *Bioresource Technololy.*, 216, 203–210.

[4] Yagub, M. T., Sen, T. K., Afroze, S., and Ang, H. M. (2014). Author’ s Personal Copy Dye and its Removal from Aqueous Solution by Adsorption: A Review. *Advances in Colloid and Interface Science 209 (2014) 172–184 Contents.* http://dx.doi.org/10.1016/j.cis.2014.04.002

[5] Shaban, M., Abukhadra, M. R., Aslam, A., and Khan, P. (2017). Removal of Congo Red, Methylene Blue and Cr (VI) Ions from Water Using Natural Serpentine. *Journal of the Taiwan Institute of Chemical Engineers*. 0, 1–15.

[6] Mojsov, K. Andronikov, D. Janevski, A. Kuzelov, A. and Gaber, S. (2016) "the application of enzymes for the removal of dyes from textile effluents," *Advanced technologies*. 5(1);

36-41.

[7] Rafatullaha, M., Sulaimana, O., Hashima, R., & Ahmadb, Anees. (2010). Adsorption of Methylene Blue on Low-Cost Adsorbents: A Review. *Journal of Hazardous Materials journal*. 177 70–80

[8] Üner, O., Geçgel, Ü., Kolancılar, H., Bayrak, Y., Kolancılar, H., and Bayrak, Y. (2017). Adsorptive Removal of Rhodamine B with Activated Carbon Obtained from Okra Wastes. *Chemical Engineering Communications*. *6445*(4).772-783.

[9] Schouten, N., Van Der Ham, L. G. J., Euverink, G-J. and Haan, A. B. (2007). Selection and evaluation of adsorbents for the removal of anionic surfactants from laundry rinsing water. Water Research, 41: 4233 – 4241.

[10] Zsilák, Z., Fónagy, O., Szabó-Bárdos, E., Horváth, O., Horváth, K., and Hajós, P. (2014). Degradation of industrial surfactants by photocatalysis combined with ozonation. Environmental Science and Pollution Research, 21(19): 11126 – 11134.

[11] Aly, S. T. El-Sayed, A. M., Tharwat, K. M., Mahmoud, M.A., Khaled, A.M., Gad, A.M., Mahmoud, and A. T. (2019). Adsorption of Nile Blue Dye Using Guava Leaf Powder. *International Journal of Engineering Research and Technology (IJERT).* 8(12), 69-72.

[12] Singh, S., Parveen, N., and Gupta, H. (2018). Adsorptive Decontamination of Rhodamine-B from Water Using Banana Peel Powder: A Biosorbent. *Environmental Technology & Innovation*. (18)30241-4,

[13] Khalid, D., Amran, M., Salleh, M., Azlina, W., Abdul, W., Idris, A., and Zainal, Z. (2012). Batch Adsorption of Basic Dye Using Acid Treated Kenaf Fibre Char: Equilibrium, Kinetic and Thermodynamic Studies. *Chemical Engineering Journal*. 182, 449–457.

[14] Yunusa, U., and Ibrahim, M. B. (2020). Adsorptive Removal of Basic Dyes and Hexavalent Chromium from Synthetic Industrial Effluent: Adsorbent Screening, Kinetic and Thermodynamic Studies. *International Journal of Engineering and Manufacturing*. (8) 54–74. https://doi.org/10.5815/ijem.2020.04.05

[15] Dabrowski, A. (2001). Adsorption from Theory to Practice. *Advanced in Colloid and Interface Science*; 93(1-3): 135-224.

[16] Mokif, L.A. (2019). Removal Methods of Synthetic Dyes from Industrial Wastewater: A

review. Mesopotamia Environmental Journal ; 5(1), 23 – 40. doi : http://dx.doi.org/10.31759/mej.2019.5.1.0040

[17] Akter, M., Bin, F., Rahman, A., Abedin, M. Z., & Kabir, S. M. F. (2021). Adsorption Characteristics of Banana Peel in the Removal of Dyes from Textile Effluent. *Textiles*; 361–375. https:// doi.org/10.3390/textiles1020018

[18] Garg, V.K. Gupta R. Yadav, A.B Kumar, R., Dye removal from aqueous solution by adsorption on treated sawdust, Bioresour. Technol. 89 (2003) 121–124.

[19] Namane, A. Mekarzia, K. Benrachedi, N. Belhaneche-Bensemra, A. Hellal, Determination of the adsorption capacity of activated carbon made from coffee grounds by chemical activation with ZnCl2 and H_3PO_4, J. Hazard. Mater. B 119 (2005) 189–194.

[20] Dutta, S., Gupta, B., Srivastava, S. K., & Gupta, A. K. (2021). Materials Advances Recent Advances on the Removal of Dyes from Wastewater Using Various Adsorbents: A Critical. *Royal society of Chemistry* 4497–4531. https://doi.org/10.1039/d1ma00354b

[21] Kamatou, G. P. P., Vermaak, I., and Viljoen, A. M. (2011). An Updated Review of Adansonia digitata: A commercially Important African Tree. *South African Journal of Botany*, 77(4), 908–9

[21] Vadivelan, V., and Kumar, K. V. (2005). Equilibrium, Kinetics, Mechanism, and Process Design for the Sorption of Methylene Blue onto Rice Husk. *Journal of Colloid and Interface Science* 286, 90–100. Doi: 10.1016/j.jcis.2005.01.007

[23] Haque, E., Jun, J. W., and Jhung, S. H. (2011). Adsorptive Removal of Methyl Orange and Methylene Blue from Aqueous Solution with a Metal-Organic Framework Material, Iron Terephthalate *(MOF-235)*. *Journal of Hazardous Materials*. *185*, 507–511. https://doi.org/10.1016/j.jhazmat.2010.09.035

[24] Hameed, B. H., & Ahmad, A. A. (2009). Batch Adsorption of Methylene Blue from Aqueous Solution by Garlic Peel, an Agricultural Waste Biomass. *Journal of Hazardous Materials*. *164*, 870–875. https://doi.org/10.1016/j.jhazmat.

[25] Pam, A. A., and Abdullah, A. H. (2022). Physicochemical Properties of Porous Activated Carbon Prepared from Palm Kernel Shell through a Low-Cost Activation Protocol. *African Journal of Science*s. *118*(9), 1–7. https://doi.org/10.17159/sajs.2022/13497 1

[26] Of, O. (2017). Preparation of Date Seed Activation for Surfactant Recovery. *Malaysian Journal of Analytical Science.* 21, (5) 1045 - 1053.

[27] Adeyi, O. (2010). Proximate Composition of Some Agricultural Wastes in Nigeria and their Potential use in Activated Carbon Production. *Journal of Applied Science Environmental Management*. 14(1) 55 - 58.

[28] Amran, M., Salleh, M., Khalid, D., Azlina, W., Abdul, W., and Idris, A. (2011). Cationic and Anionic dye Adsorption by Agricultural Solid Wastes: A Comprehensive Review. *Desalination; 280*, 1–13.

[29] Ohimor, E. O., Temisa, D. O., and Ononiwu, P. I. (2021). Production of Activated Carbon from Carbonaceous Agricultural Waste Material: Coconut Fibres. *Nigerian Journal of Technology*. 40,(1) 19–24.

[30] Ekpete, O. A., Marcus, A. C., and Osi, V. (2017). Preparation and Characterization of Activated Carbon Obtained from Plantain (Musa Paradisiaca) Fruit Stem. *Journal of Chemistry*. (1):1-6.

[31] Sugumaran, P., Susan, V. P., Ravichandran, P., and Seshadri, S. (2012). Production and Characterization of Activated Carbon from Banana Empty Fruit Bunch and Delonix regia Fruit Pod. *Journal of Sustainable Energy & Environment. 3*, 125–132.

[32] Ences, S., Renou, J.G., Givaudan, S., Poulain, F., Dirassouyan, & Moulin, P., (2008). Landfill leachate treatment: Review and opportunity, Journal of *Hazardous Material*. 150 468–493.

[33] Benı ´tez, S.O. J.L.B. Lozano, The municipal solid waste cycle in Mexico: Final disposal, Res, C. E. J. 150 (2009) 174–180. (2017). Kinetic Modeling of Liquid-Phase Adsorption of Congo Red Dye Using Guava Leaf-Based Activated Carbon. *Applied Water Science*, *7*(4), 1965–1977. https://doi.org/10.1007/s13201-015-0375-y

[34] Kamaru, A. A., Sani, N. S., Ahmad, N., and Nik, N. (2015). Raw and Surfactant-Modified Pineapple Leaf as Adsorbent for Removal of Methylene Blue and Methyl Orange from Aqueous Solution. *Desalination and Water Treatment 3994*(11), 0–15. https://doi.org/10.1080/19443994.2015.1095122

[35] Sajid, M., Javed, T., Areej, I., and Nouman, M. (2022). Sequestration of Crystal Violet

Dye from Wastewater Using Low-Cost Coconut Husk as a Potential Adsorbent. *Water Science and Technology*. *85*(8), 2295–2317. https://doi.org/10.2166/wst.2022.124

[36] Sharma, S. and Kaur, A. (2018) Various methods for removal of dyes from industrial effluents-a review. *Indian Journal of Science and Technology* 11,1–21.

[37] Tariq, J., Nasir, K. and Mirza, M. L. 2017 Kinetics, Equilibrium and Thermodynamics of Cerium Removal by Adsorption on Low-Rank Coal. *Desalination and Water Treatment.* 89, 240–249.

[38] Chinniagounder, T., Shanker, M. and Nageswaran, S. (2011). Adsorptive Removal of Crystal Violet Dye Using Agricultural Waste Cocoa (Theobroma cacao) Shell. R*esearch Journal of Chemical Sciences* 2231, 606X.

[39] Nasar, A. and Shakoor, S. (2018) Remediation of Dyes from Industrial Wastewater using Low-Cost Adsorbents. *Materials Research Foundations*. 15, 1–33. doi: http://dx.doi.org/10.21741/9781945291333-1.

[40] Fu, F., Gao, Z., Gao, L., and Li, D. (2011). Effective Adsorption of Anionic Dye, Alizarin Red S, from Aqueous Solutions on Activated Clay Modified by Iron Oxide. *Industrial and Engineering Chemistry Research*; 50(16) 9712–9717.

[41] Senthamarai, C., Senthil-Kumar, P., Priyadharshini, M., Vijayalakshmi, P., Vinoth-Kumar, V., Baskaralingam, P., Tiruvengadaravi, K.V., Sivanesan, S. (2012). Adsorption behavior of methylene blue dye onto surface modified Strychnos potatorum seeds. Environ Prog Sust Energ 2012;32(3):624–32.

[42] Ences, S., Renou, J.G., Givaudan, S., Poulain, F., Dirassouyan, & Moulin, P., (2014). Landfill leachate treatment: Review and opportunity, Journal of *Hazardous Material*. 150 468–493.

[43] Bhattacharyya, K.G. Gupta, S.S. (2006) Adsorption of Fe(III) from Water by Natural and acid activated Clays: Studies on equilibrium Isotherm, Kinetics and Thermodynamics of Interactions. Adsorption 12,185-204 2006. https://dio.org/10.1007/s10450-006-0145-0

[44] Vasudevan, S., and Alothman, Z. A. (2015). Adsorption Kinetics, Isotherms, and Thermodynamic Studies for Hg Adsorption from Aqueous Medium using Alizarin Red-S-Loaded Amberlite IRA-400 Resin. *Desalination and Water Treatment*. (1) 1-9.

[45] Marie, A., Atia, A.A., Elgogary, T.M., and El-Nashas, A.M. (2019). Adsorption of Cu^{2+} and Mg^{2+} Ions on Silica Gel Derived from Rice Hulls ash: Experimental and Theoretical Studies. *Journal of Theoretical and Computational Chemistry*, 18(5), 1950026. https://doi.org/10.1142/50219633619500263

[46] Khalfaoui, A., Khelifi, M. N., Khelfaoui, A., Benalia, A., & Derbal, K. (2022). The Adsorptive Removal of Bengal Rose by Artichoke Leaves: Optimization by Full Factorials Design. *Water*. https://doi.org/10.3390/w14142251

[47] Zakaria, R., Jamalluddin, N. A., and Abu Bakar, M. Z. (20121). Effect of impregnation ratio and activation temperature on the yield and adsorption performance of mangrove based activated carbon for methylene blue removal. *Results in Materials*; 10(3), 100-183. https://doi.org/10.11016/j.rinma.2021.100183

[48] Zubair, M., Dalhat, N., Jarrah, N., & Blaisi, N. I. (2020). Adsorption Behavior and Mechanism of Methylene Blue, Crystal Violet, Eriochrome Black T, and Methyl Orange Dyes onto Biochar-Derived Date Palm Fronds Waste Produced at Different Pyrolysis Conditions. *Water Air Soil Pollution*. https://doi.org/10.1007/s11270-020-04595-x

[49] Sultana, S., Islam, K., Hasan, M. A., Khan, H. J., Khan, M. A. R., Deb, A., Al Raihan, M. and Rahman, M. W. (2022). Adsorption of Crystal Violet Dye by Coconut Husk Powder: Isotherm, Kinetics and Thermodynamics Perspectives. *Environmental Nanotechnology, Monitoring & Management*. 17(9): 100651

[50] Kumar, K. Y., Muralidhara, H. B., Nayaka, Y. A., Balasubramanyam, J., and Hanumanthappa, H. (2013). Low-Cost Synthesis of Metal Oxide Nanoparticles ond their Application in Adsorption of Commercial Dye and Heavy Metal Ion in Aqueous Solution. *Powder Technology*, 246, 125–136.

[51] Bashir, M., Mohammed, S. Y, Atiku, M. K, Bello, A. U., and Yakasai, H. A. (2021). Heavy Metals Content in Laboratory Wastewater: A Case Study of Selected Units of Bayero University, Kano-Nigeria. *Bayero Journal of Pure and Applied Sciences 14*(2), 174–177. http://dx.doi.org/10.4314/bajopas.v14i2.20

[52] Singh, S., Parveen, N., & Gupta, H. (2018). Adsorptive Decontamination of Rhodamine-B from Water Using Banana Peel Powder: A Biosorbent. *Environmental*

Technology & Innovation. (18)30241-4, https://doi.org/10.1016/j.eti.2018.09.001

[53] Imam, S. S., and Babamale, H. F. (2020). A Short Review on the Removal of Rhodamine B Dye using Agricultural Waste-Based Adsorbents. *Asian Journal of Chemical Sciences*. *7*(1), 25–37. https://doi.org/10.9734/AJOCS/2020/v7i119013